VARIATIONAL METHODS AND SPEED-UP OF MONTE CARLO PERTURBATION COMPUTATIONS FOR OPTIMAL DESIGN IN NUCLEAR SYSTEMS

by

Zafar Ullah KORESHI [1*]***, Hamda KHAN*** [2]***, and Muhammad YAQUB*** [3]

[1] Department of Mechatronics Engineering, Air University, Islamabad, Pakistan
[2] Department of Mathematics, National University of Computer and Emerging Sciences, Islamabad, Pakistan
[3] Department of Mathematics, Riphah International University, Islamabad, Pakistan

Scientific paper
http://doi.org/10.2298/NTRP190214032K

Seeking optimal material distribution in a nuclear system to maximize a response function of interest has been a subject of considerable interest in nuclear engineering. Examples are the optimal fuel distribution in a nuclear reactor core to achieve uniform burnup using minimum critical mass and the use of composite materials with an optimal mix of constituent elements in detection systems and radiation shielding. For such studies, variational methods have been found to be useful but, they have been used for standalone analyses often restricted to idealized models, while more elaborate design studies have required computationally expensive Monte Carlo simulations ill-suited to iterative schemes for optimization. Such an inherent disadvantage of Monte Carlo methods changed with the development of perturbation algorithms but, their efficiency is still dependent on the *reference* configuration for which a hit-and-trial approach is often used. In the first illustrative example, this paper explores the computational speedup for a bare cylindrical reactor core, achievable by using a variational result to enhance the computational efficiency of Monte Carlo design optimization simulation. In the second example, the effect of non-uniform material density in a fixed-source problem, applicable to optimal moderator and radiation shielding, is presented. While applications of this work are numerous, the objective of this paper is to present preliminary variational results as inputs to elaborate stochastic optimization by Monte Carlo simulation for large and realistic systems.

Key words: variational method, optimal distribution, Monte Carlo perturbation, nuclear system, minimum critical mass

INTRODUCTION

The objective of distributing materials in a nuclear system, multiplying or fixed-source, is to maximize (or minimize) some quantity of interest such as minimizing the fissile mass in a nuclear fission reactor, maximizing the tritium production in a fusion blanket, or minimizing the radiation environment surrounding a detection system. Thus, optimal distributions lie at the heart of design optimization for which variational methods [1-5] are extensively used although often for idealized configurations. Further, in design optimization, sensitivity coefficients due to uncertainty in nuclear cross-section data, material and geometric perturbation [6-9] can also be determined with variational methods. Good computational efficiency has been achieved for large-scale reactor design computations and with diverse applications in engineering [10]. For the optimal arrangement of fuel in a core, the Pontryagin Maximum Principle is used [3], to estimate the *optimal control*, *i. e*., best placement of high and low enriched fuel in the core. This constitutes an ODE-constrained optimization problem with the diffusion equation as the *constraint*. The drawback with variational methods has been their difficulty to be applied for large problems, for which Monte Carlo methods [11-13] and heuristic methods such as genetic algorithms have been demonstrated to be more attractive [14]. However, variational methods have been extended [7-9, 15] to thermal reactor physics calculations, with the computationally accelerated 3-D heterogeneous variational node method, amenable to parallelization. In the Monte Carlo method, sensitivity coefficients can be estimated by obtaining *derivatives* sampled in a single run thus, avoiding the need for performing an *adjoint* run in addition to a *forward* run, as is done in the deterministic approach. However, derivative sampling has been found to be accurate for small

* Corresponding author; e-mail: zafar@mail.au.edu.pk

perturbations and hence, the choice of a *reference* condition has bearings on the computational efficiency of an optimization simulation. This work explores the computational advantage of using a variational result as *an educated guess* for starting a Monte Carlo derivative sampling simulation. Initial variational results are obtained from two-group neutron diffusion equations for illustrative examples of a two-zone reactor core, and a non-multiplying medium. In the formulation of this *optimal control* problem with the material density as the *control variable*, the Lagrangian is used since the effect of material distribution on the response of interest has a direct and an indirect component. The former due to the material density change and the latter due to the change in the field function *i*. *e*., the neutron flux, due to the change in density. As an example, the two-group theory is *matched* with the detailed MCNP5 [16] simulation results to strengthen its validity and enable its use to generalize on the applicability of its results.

This work presents a useful insight into the different approaches and is applicable to design optimization in nuclear systems.

VARIATIONAL FORMULATION

In design optimization, one of the goals is to maximize some reaction rate, or performance index, R_{k} $\Sigma_{\mathrm{k},}\underline{\phi}$ subject to a constraint such as the neutron diffusion (or transport) equation

$$\hat{M}\underline{\phi} \quad 0 \tag{1a}$$

In a *two-group* formulation [17]

$$\hat{M} \quad \begin{matrix} \hat{L}_1 & \nu\Sigma_{f,2} \\ p\Sigma_{s,1\ 2} & \hat{L}_2 \end{matrix} \tag{1b}$$

Here we have assumed that fission neutrons are produced in the thermal group (group 2) and appear in the fast group (group 1). The atomic density of the materials, for a non-uniform distribution, can be written as $N(x) = f(x)N_{\mathrm{o}}$, subject to $\int_a^b f(x)\mathrm{d}x \quad 1$ in some domain $\Gamma \quad (a,b)$ with appropriate boundary conditions. In eq. 1(a), the flux vector is $\underline{\phi} \quad [\phi_1, \phi_2]^T$ and the operator is $\hat{L}_{\mathrm{g}} \quad D_{\mathrm{g}} \ \phi_{\mathrm{g}} \quad \Sigma_{\mathrm{r,g}}\underline{\phi}_{\mathrm{g}} \ (g \quad 1,2)$.

The variational formulations considered here have a *continuous* control u, and a discrete control u having an admissible set of values corresponding to the minimum and maximum values $u_{\min}$ and $u_{\max}$, respectively.

In the *continuous formulation*, the Lagrangian is written as

$$\mathcal{L} \quad R_k \quad \underline{\phi}^{\ T}, \ \hat{M}\underline{\phi} \tag{2}$$

with an objective to obtain the optimal distribution u^* by seeking first-order variations for a stationarity condition.

In the *discrete* formulation, where the control is given a value, the equations become easier to solve. Then eq. 1(a) is written in state-space form for variables y_i expressed as

$$\dot{y}_i \quad f_i(\underline{y},u,x), i \quad 0,1,2,3,4 \tag{3}$$

with the performance index included.

The Hamiltonian is then written as

$$H \quad \sum_{i\ 0}^{4} \lambda_i f_i(\underline{y},u,x) \tag{4}$$

which yields the stationarity conditions

$$\dot{y}_i \quad f_i(\underline{y},u,x) \quad \frac{\partial H}{\partial \lambda_i} \tag{5a}$$

and the *adjoint* equations

$$\dot{\lambda}_t \quad \frac{\partial H}{\partial y_i} \tag{5b}$$

With solutions obtained for y_i and λ_i, using the transversality boundary conditions, the Hamiltonian can be found in the form

$$H \quad g(u,x) \quad h(x) \tag{6}$$

and thus the shape of $g(u, x)$, also refered to as the *switching function*, determines which of the admissible values of the control u are to be applied to maximize H. Then, according to Pontryagin's Maximum Principle

$$H(\underline{y}^*,u^*,x) \quad H(\underline{y}^*,u,x) \tag{7}$$

where $u_{\min} \quad u \quad u_{\max}$.

We now consider two illustrative examples where the previous formulations are used to obtain optimal distributions.

EXAMPLE 1: OPTIMAL FUEL ENRICHMENT

In a nuclear reactor core, fuel of varying enrichment is used and placed in such a way that uniform burnup is achieved and minimum fuel is required for criticality. The optimization problem is thus formulated as follows: Given some maximum fuel enrichment $u_{\max}$, what is the *best* placement of fuel such that the reactor is critical with minimum fuel mass? This is formulated as follows: minimize $R = < u >$ where $u \quad {}_2 \ \gamma u \quad \delta, \gamma \quad \sigma_a^{235} N^{235}, u \quad N^5 / N^U$ (enrichment), $\delta = N^{\mathrm{others}} \sigma_{\mathrm{a}}^{\mathrm{others}}$ with the constraint of fixed N^U – total number of uranium atoms in the domain $r \quad (0, R)$ subject to the constraint of eq. 1(a) with appropriate boundary conditions [3]. For a bare cylindrical reactor, the coupled second-order ODE representing the governing equation $\hat{M}\underline{\phi} \quad 0$ are written in state space form with the variables $y_1 = \phi_1$, $y_2 = r\,\mathrm{d}\phi_1/\mathrm{d}r$, $y_3 = \phi_2$, and $y_4 = r\,\mathrm{d}\phi_2/\mathrm{d}r$. The first-order equations are then

$r\dot{y}_1 \quad y_2, \tau_1 \dot{y}_2 \quad ry_1 \quad \tau_1 \alpha u r y_3, r\dot{y}_3 \quad y_4$, and $\tau_2 \dot{y}_4 \quad ry_1 \quad \tau_2 \beta u r y_3$ with $\dot{y}_0 \quad 2\pi u r$ added as a state equation. Here, $\tau_1 \quad D_1 / \ _1, \tau_2 \quad p \ _1 / D_2$, $\alpha \quad k_\infty / pD_1^{'}, \beta \quad 1/D_2$

These equations are solved using the transversality boundary conditions

$$\lambda_i(R)\delta y_i(R) \quad \lambda_i(0)\delta y_i(0) \quad 0 \qquad (8)$$

for which the flux boundary conditions $\phi_1^{'}\big|_{r \ 0} \quad \phi_2^{'}\big|_{r \ 0} \quad 0$ and $\phi_1\big|_{r \ R} \quad \phi_2\big|_{r \ R} \quad 0$, yield boundary conditions for the adjoint fluxes: $\lambda_1\big|_{r \ 0} \quad \lambda_3\big|_{r \ 0} \quad 0$ and $\lambda_2\big|_{r \ R} \quad \lambda_4\big|_{r \ R} \quad 0$.

The Hamiltonian is now written in the form of eq. (6) with

$$g(u,r) \quad u(2\pi r\lambda_0 \quad \alpha r\lambda_2 y_3 \quad \beta r\lambda_4 y_3) \qquad (9a)$$

and

$$h(r) \quad \frac{1}{r}\lambda_1 y_2 \quad \frac{1}{\tau_1} r\lambda_2 y_1 \quad \frac{1}{r}\lambda_3 y_4 \quad \frac{1}{\tau_2} r\lambda_4 y_1 \qquad (9b)$$

and thus the shape of $g(u)$, also refered to as the *switching function*, determines which of the admissible values of the control u are to be applied according to Pontryagin's Maximum Principle where $u_{\min} \quad u \quad u_{\max}$.

The discrete form simplifies the continuous form by permitting the control u to be a constant in a particular sub-domain of the problem. Thus where $g(u, x)$ is minimum (either sign), $u_{\max}$ is applied and vice versa. The number of zeros of the switching function will determine the number of controls applied. At the boundaries, $g(u, 0) = 0$, and $g(u, R) < 0$ with zeros in between. It can be inferred [3] that for the two-zone case, H is maximized with $u = u_{\max}$ in the first zone $0 < r \quad R_1$ and $u = u_{\min}$ in the second zone $R_1 < r \quad R$ where the zone boundary is at $r = R_1$. While contrary to engineering practice of lower enrichment in the inner zone, this example is presented merely to demonstrate an optimal result. Similarly, for three zones, the maximization requirement is the control strategy $u_{\min}, u_{\max}, u_{\min}$ for the first, second and third zones, respectively. We thus need to find the critical pairs for each permissible value of $u \quad u_{\max}$. This is achieved from the criticality condition found by solving for the two-group fluxes using Cramer's rule ($\det(\Psi) = 0$) for homogenous equations. For the one- and two-zone cases, the conditions are:

One zone

$$\begin{vmatrix} S_{11}J_0(\mu R) & S_{13}I_0(\lambda R) \\ J_0(\mu R) & I_0(\lambda R) \end{vmatrix} \quad 0 \qquad (10a)$$

Two zone

$$\begin{vmatrix} \mu_I S_{11}J_1(\mu_1 r_1) & \mu_2 S_{21}J_1(\mu_2 r_1) & \mu_2 S_{22}Y_1(\mu_2 r_1) & \lambda_1 S_{13}I_0(\lambda_1 r_1) & \lambda_2 S_{23}I_1(\lambda_2 r_1) & \lambda_2 S_{24}K_1(\lambda_2 r_1) \\ \mu_1 J_1(\mu_1 r_1) & \mu_2 J_1(\mu_2 r_1) & \mu_2 Y_1(\mu_2 r_1) & \lambda_1 I_1(\lambda_1 r_1) & \lambda_2 I_1(\lambda_2 r_1) & \lambda_2 K_0(\lambda_2 r_1) \\ S_{11}J_0(\mu_1 r_1) & S_{21}J_0(\mu_2 r_1) & S_{22}Y_0(\mu_1 r_1) & S_{13}I_0(\lambda_1 r_1) & S_{23}I_1(\lambda_2 r_1) & S_{24}K_0(\lambda_2 r_1) \\ J_0(\mu_1 r_1) & J_0(\mu_2 r_1) & Y_0(\mu_1 r_1) & I_0(\lambda_1 r_1) & I_0(R_2 r_1) & K_0(\lambda_2 r_1) \\ 0 & S_{21}J_0(\mu_2 R) & S_{22}Y_0(\mu_2 R) & 0 & S_{23}I_0(\lambda_2 R) & S_{24}K_0(\lambda_2 R) \\ 0 & J_0(\mu_2 R) & Y_0(\mu_2 R) & 0 & I_0(\lambda_2 R) & K_0(\lambda_2 R) \end{vmatrix} \quad 0 \qquad (10b)$$

Where J_0, Y_0 are Bessel functions of order zero of first and second kind, and I_0, K_0 are modified Bessel functions of the first and second kind, respectively. Here, S_{ij} are the coupling coefficients for zone i and index j with

$$S_{11} \quad \tau_2(\mu^2 \quad \beta u) \quad S_{21} \quad S_{22}$$
$$S_{13} \quad \tau_2(\lambda^2 \quad \beta u) \quad S_{23} \quad S_{24}$$
$$\mu^2 \quad \frac{1}{2\tau_1 L^2}[\ (\tau_1 \quad L^2) \quad \sqrt{(\tau_1 \quad L^2)^2 \quad 4(k_\infty \quad 1)\tau_1 L^2}$$
$$\lambda^2 \quad \frac{1}{2\tau_1 L^2}[(\tau_1 \quad L^2) \quad \sqrt{(\tau_1 \quad L^2)^2 \quad 4(k_\infty \quad 1)\tau_1 L^2}$$

For the three-zone case, Lee [3] has obtained a $10 \times$ determinant.

We consider a bare homogeneous nuclear reactor core (radius 122.6 cm, height 365.8 cm) with the following two-group data [17]

$$D_1 = 1.13 \text{ cm}, \Sigma_s = 0.0419 \text{ cm}^{-1}$$
$$D_2 = 0.16 \text{ cm}, \sigma_a^{235} \quad 678\, b$$
$$N^U \quad \mathrm{N}^{235} \quad \mathrm{N}^{238} \quad 6.994\ 10^{21} \text{ atoms per cm}^3$$

Clearly, no *optimal* arrangement can be determined from the one-zone case as the bare reactor is found to be critical for a uniform enrichment of 1.1 % (critical mass 518.7 kg U^{235}). For a two-zone equal-volume (R = 86.6913 cm, 122.6 cm) configuration, the critical enrichment pairs found from the determinant are given in tab. 1. As the fuel enrichment in the first zone increases from natural uranium ($u_{\max}$ = 0.71 %) to 1.2 %, the enrichment decreases in the second zone. With these combinations, the average u (a measure of the minimum critical mass) is given in the third row while MCNP results are given in the fourth row.

Table 1. Two-zone enrichment pairs for criticality

u_{max}/u_1	0.71	0.9	1.1	1.2
u_{min}/u_2	1.54	1.27	1.1	1.01
u_{av}	1.13	1.09	1.1	1.13
MCNP	0.96760 (0.00397)	0.96538 (0.00190)	1.00422 (0.00192)	1.03035 (0.00169)

Table 2. Critical pairs, relative critical mass, MCNP runs

Zone 1	DTPMP		MCNP (500 1 10 500)*
	u_{min} [%]	RCM	
1.14	1.040	0.9797	1.00982 (0.00104)
1.13	1.042	0.9869	1.00950 (0.00097)
1.12	1.053	0.9869	1.00628 (0.00101)
1.11	1.067	0.9914	1.00447 (0.0010)
1.10	1.087	1.0	1.00419 (0.00191)

* (500 1 10 500) – means 500 neutrons simulated with an eigenvalue guess of 1 for 500 cycles with 10 skip cycles

There are no solutions for u_{max} 1.2 because at an enrichment of 1.2 %, the critical radius is less than the radius of the first zone. The MCNP runs for 1000 neutrons per cycle and 100 cycles give a preliminary estimate of k_{eff} = 1.00195 (0.00190) for 1.2 % enrichment with a bare cylindrical reactor of radius 68.05 cm and height 365.80 cm. The feasible solution for an optimal is thus the range 1.1-1.2 % enrichment in the first zone.

Two-group criticality pairs found from eq. 10(b) are given in tab. 2 along with the relative critical masses and corresponding MCNP simulations for 500 neutrons per cycle for 500 cycles and 10 skip cycles.

Assuming that the maximum available enrichment is 1.14 %, the minimum relative critical mass found is 0.9797 (508.18 kg U^{235}).

The masses in both zones are related as follows

$$M_2^{235} \quad \frac{u_1 V_1}{u_2 V_2} M_1^{235}$$

so that the relative critical mass (RCM) is defined as

$$\text{RCM} \quad \frac{M_1^{235} \quad M_2^{235}}{M_0^{235}} \quad \frac{u_1 \quad u^2}{u_1} \frac{M_1^{235}}{M_0^{235}}$$

where M_i^{235} mass of U^{235} in zone 1, u_i = enrichment in zone 1, V_i = volume of zone 1, M_0^{235} mass of U^{235} in zones 1 and 2 for 1.1 % uniform distribution (518.7 kg).

The problem with increased enrichment in the central core is the enhanced fuel peaking which is not desirable and hence, less enriched fuel is placed in the central core. The present result is correct within the limitations of the two-zone model considered. Here, the total mass increases as lower enriched fuel is placed in the central core, as shown in fig. 1.

Figure 2 shows the thermal fluxes obtained from MCNP for three cases *viz* 1.1 % uniform enrichment, and

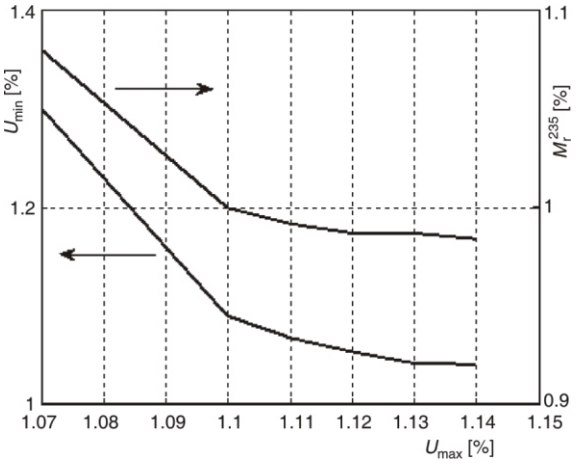

Figure 1. Minimum critical mass for a two-zone reactor

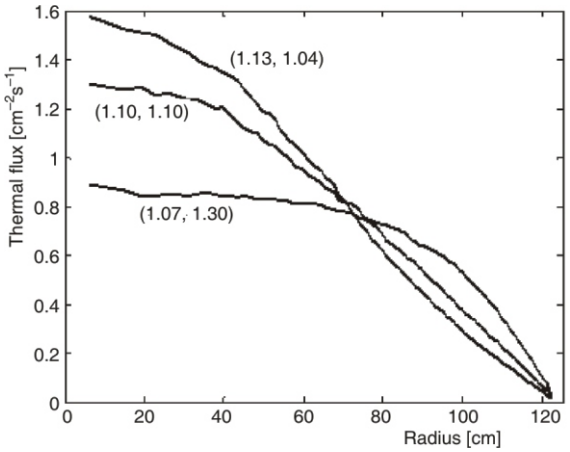

Figure 2. Thermal flux shape in reactor

small perturbations: 1.07 %-1.3 % and 1.13 %-1.04 % enrichments showing clearly the flattening of the thermal flux with a lower inner zone enrichment.

The criticality pairs can be computed from MCNP simulations by carrying out runs for each case which is clearly computationally expensive. This can be avoided by using the perturbation capability of MCNP5 [11] for sampling first- and second-order derivatives in a two-term Taylor series which can be used to estimate k_{eff} for perturbations in the enrichment in terms of a reference $k_{eff}(u_o)$

$$k_{eff}(u) \quad k_{eff}(u_0) \quad \frac{dk_{eff}}{du}\Big|_{u_0} \delta u$$
$$\frac{1}{2!} \frac{d^2 k_{eff}}{du^2}\Big|_{u_0} (\delta u)^2 \quad \ldots$$

This formulation is suitable for optimization analyses which require the ability to estimate the effect of small changes such as in material density or geometry.

Thus, the first derivatives is computed as

$$c_1 \quad \frac{dk_{eff}}{du}\Big|_{u_0} \quad \frac{k_{eff}(u) \quad k_{eff}(u_0)}{\delta u} \quad \frac{\delta k}{\delta u}$$

and the second derivative as

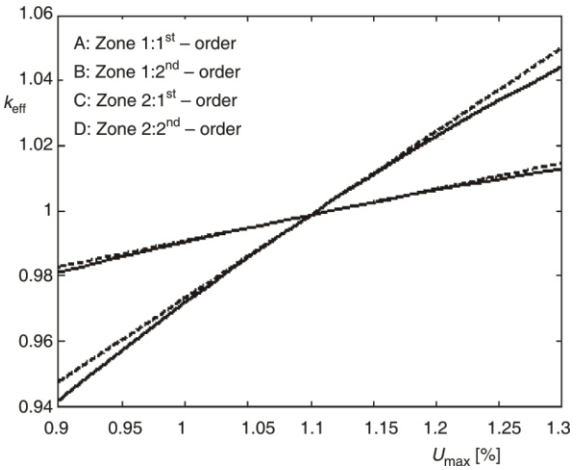

Figure (3a). Perturbation estimates for k_{eff}

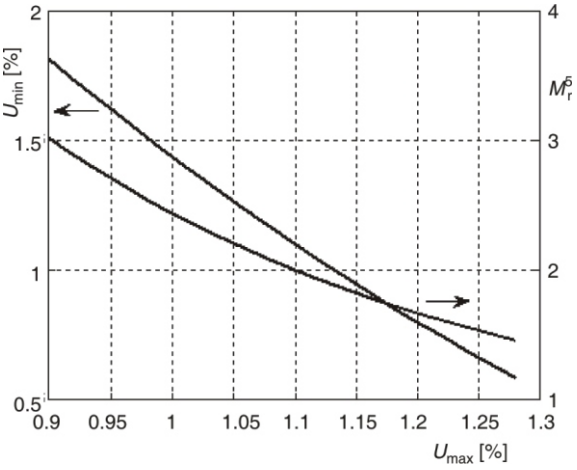

Figure (3b). Criticality pairs predicted by perturbation

$$c_2 \quad \frac{\mathrm{d}^2 k_{\text{eff}}}{\mathrm{d}u^2}\Big|_{u_0} \quad 2\frac{k_{\text{eff}}(u) \quad k_{\text{eff}}(u_0) \quad c_1\delta u}{(\delta u)^2}$$

$$2\frac{\dfrac{\delta k}{\delta u}^{(2)} \quad \dfrac{\delta k}{\delta u}^{(1)}}{\delta u}$$

where $(\delta k/\delta u)^{(1,2)}$ are the quantities estimated from first- and second-order derivatives, respectively. Since the validity of perturbation theory is limited to small perturbations, the reference condition is important for a criticality search in a close neighbourhood. Such a reference is used from the variational results of tab. 1.

The first and second derivatives are estimated as 0.2563 and –0.2889 for zone 1, and 0.0800 and –0.0857 for the second zone, respectively. These are used to predict k_{eff} for enrichment perturbations shown in fig. 3(a). Thus, an increase in fuel enrichment in zone 1 is balanced by a decrease in enrichment in zone 2 so that the net effect gives k_{eff}~1 which leads to the criticality pairs predicted as shown in fig. 3(b).

The results are accurate to within 1 % while the computational effort is reduced due to derivatives collected in a single run.

Further, the *good* reference condition provided by preliminary variation results show that estimates from both first- and second-derivatives, labelled FS for zones 1 and 2 in fig. 3(a), are only slightly better than the first derivative estimates, labelled F.

The previous analysis can readily be extended to three zones for which Pontryagin's Maximum Principle gives a $u_{\min}$, $u_{\max}$, $u_{\min}$ which agrees better with Goertzel's condition for flat thermal flux, as being the condition for minimum critical mass according to diffusion theory. The results for the two-zone case are to illustrate the variational formulation which gives a maximum value for the Hamiltonian (eq. 7) for a $u_{\max}$, $u_{\min}$ configuration.

EXAMPLE 2: NON-UNIFORM DENSITY IN A FIXED SOURCE SYSTEM

Similar to the previous example, in a fixed-source nuclear system, non-uniform material density may be considered for both elements and mixtures (with constituent elements) with the objective of increasing some reaction rate or decreasing the size of the system. For such an optimization problem, it would be desirable to obtain the optimal material distribution. Such a problem could use the continuous form of the variational formulation. With $R_k \quad {}_k, \underline{\phi}$ and ${}_k \quad N(x)\sigma_k \quad u(x)\sigma_\kappa$ the Lagrangian is

$$\mathcal{L} \quad u\sigma_x^T, \underline{\phi} \qquad \underline{\phi}^T, \hat{M}\underline{\phi} \tag{11}$$

with an objective to obtain the optimal distribution u^* by seeking first-order variations for a stationarity condition.

With variations in $u, \underline{\phi}, \underline{\phi}$ and $\hat{M}$ and requiring the variations in the trial functions to be zero in the domain (excluding the boundary) we get for slab geometry

$$\hat{L}_1\phi_1 \quad u(x)\sigma_{r,1}\phi_2 \quad 0 \tag{12a}$$

$$\hat{L}_2\phi_{21} \quad u(x)\sigma_x \quad 0 \tag{12b}$$

$$^2_{t\ 1}\frac{1}{3\sigma_{tr,i}} \quad \frac{1}{N}\frac{d}{\mathrm{d}x}\frac{1}{N}\frac{\mathrm{d}\phi_i}{\mathrm{d}x} \quad \phi_i$$

$$\frac{d}{\mathrm{d}x}\frac{1}{N^2}\frac{\mathrm{d}\phi_i}{\mathrm{d}x} \quad \phi_i \qquad 0 \tag{12c}$$

The previous formula are solved to give the fluxes

$$\phi_1(x) \quad A_1 \mathrm{e}^{\gamma_1 \ u(x)\mathrm{d}x} \quad A_2 \mathrm{e}^{\ \gamma_1 \ u(x)\mathrm{d}x} \tag{13a}$$

$$\phi_2(x) \quad A_3 \mathrm{e}^{\gamma_2 \ u(x)\mathrm{d}x} \quad A_4 \mathrm{e}^{\ \gamma_2 \ u(x)\mathrm{d}x} \quad \varpi\phi_1(x) \tag{13b}$$

$$\phi_1(x) \quad A_7 e^{\gamma_1 \int u(x)dx} \quad A_8 e^{-\gamma_1 \int u(x)dx}$$

$$\phi_2(x) \quad \frac{\sigma_x}{\sigma_{r,2}} \quad \frac{\sigma_x}{\sigma_{r,2}} \tag{13c}$$

$$\phi_2(x) \quad A_5 e^{\gamma_2 \int u(x)dx} \quad A_6 e^{-\gamma_2 \int u(x)dx} \quad \frac{\sigma_x}{\sigma_{r,2}} \tag{13d}$$

where $\gamma_i \quad \sqrt{3\sigma_{r,i}\sigma_{tr,i}}$, $\varpi = \frac{\sigma_{r,1}}{\sigma_{r,2}} \quad 1 \quad \left(\frac{\omega_1}{\omega_2}\right)^{2} \quad ^{1}$, $\omega_i^2 \quad \sigma_{r,i}/3\sigma_{tr,i}$ $(i \quad 1,2)$

Equations 13(a)-13(d) can be inserted in eq. 12(c) to get the optimal distribution $u^*(x)$.

In the test problem, a slab of water thickness 20 cm is considered with a unit source of energy corresponding to group 1. In this case the *control* variable is the number density $N(x)$ subject to the constraint of fixed total material. The performance index is the (n, γ) reaction rate $R_{H\,(n,\gamma)} \quad \int_a^b N(x)\phi_2(x)dx$ in water and it is investigated whether the change in material distribution results in an optimum PI. The boundary conditions are thus

$$J_1(x \quad 0) \quad D_1 \left.\frac{d\phi_1}{dx}\right|_0 \quad \frac{S}{2}$$

and

$$\phi_1(x \quad L) \quad \phi_2(x \quad 0) \quad \phi_2(x \quad L) \quad 0$$

Validation is carried out by computing two-group fluxes for material density uniform, linearly increasing and linearly decreasing as shown in fig. 4.

For the previous three cases, results are shown in fig. 5 where the gradual rise, then fall, in the group-2 fluxes is seen.

Figure 5 shows the effect of the density on group fluxes. It is seen that both 'move towards the right' for

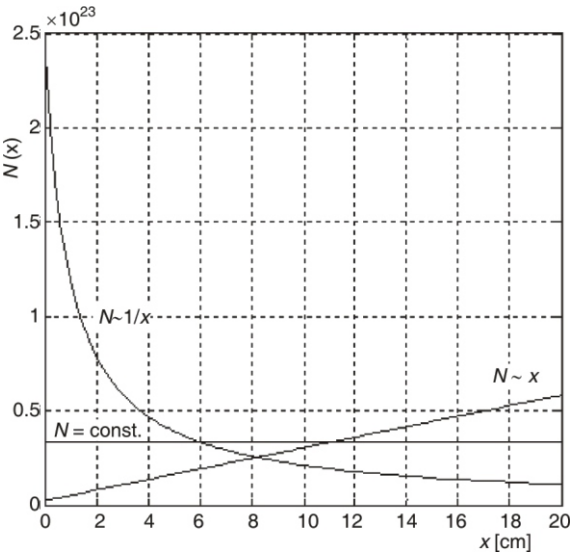

Figure 4. Material density distribution considered for uniform distribution, linearly decreasing and linearly increasing distribution

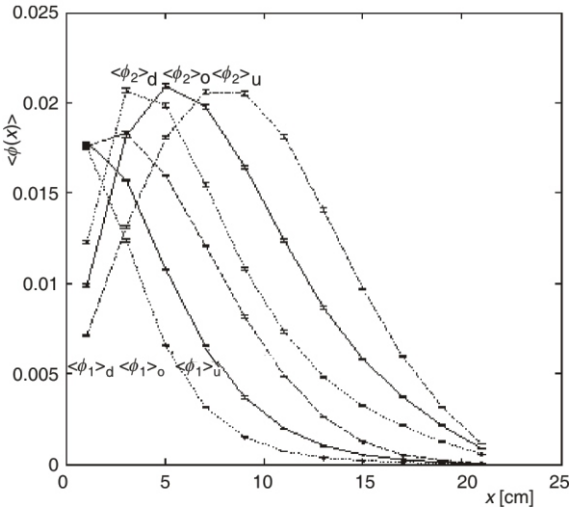

Figure 5. Neutron fluxes with MCNP5 in group 1 (E > > 5 eV) and group 2 (E 5eV), and (n, γ) reaction rate in water; $<\phi_i>$ is the *zone-averaged* neutron flux in energy group i; subscripts o, d, u refer to uniform-density, linearly decreasing, linearly increasing density

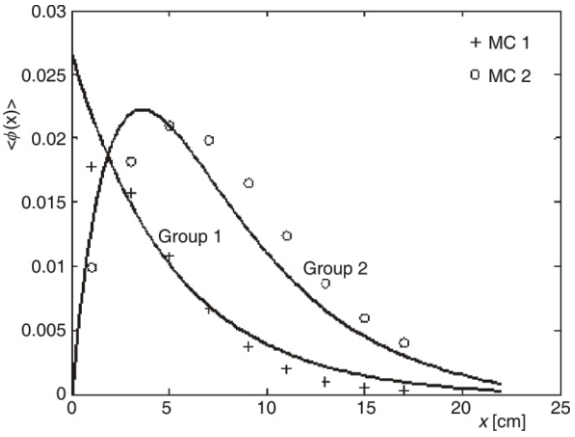

Figure 6. Neutron fluxes with two-group diffusion theory compared with MCNP in group 1 (E > 5eV) and group 2 (E 5 eV)

the case of linearly increasing material distribution. These are compared with diffusion theory results shown in fig. 6.

All three cases are shown in fig. 7 (diffusion theory fluxes), where the *left* and *right* shift of the decreasing and increasing densities is seen.

Corresponding to the three cases, the PI is shown in fig. 8 with the trend mentioned earlier, *i. e*., a gradual shift towards the right for linearly increasing density.

To estimate the currents and subsequent doses, MCNP5 simulations were carried out for a slab (20 cm 10 cm 10 cm) containing water, with a 1 MeV neutron source incident on the left face (along the +x-axis) of thickness of 20 cm. The front and back surfaces were considered to be reflecting surfaces. The quantities tallied with MCNP5 were *i*- currents (neutron F1:n and photon F11:p tallies) emitted from the right face of

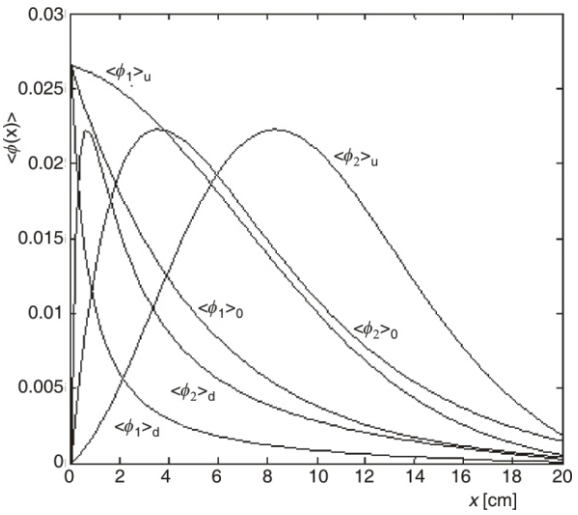

Figure 7. Neutron fluxes with two-group neutron diffusion theory in group 1 (E > 5eV) and group 2 (E 5 eV) in a slab of water with uniform, linearly decreasing and linearly increasing density

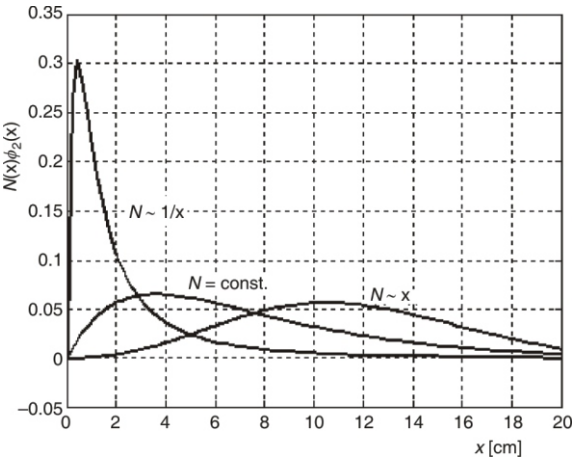

Figure 8. Performance index with two-group neutron diffusion theory in group 1 (E > 5eV) and group 2 (E 5 eV)

the slab, *ii*- dose equivalents in Sieverts (neutron and photon using dose equivalent factors), and *iii*- the reaction rates $R_H(n, \gamma)$ in cells of thickness 2 cm each in two energy bins (E_1 5 eV and 5 eV E_2 1 MeV). The results for NPS = 10^5 with a PHYS:P cutoff at 100 keV (PHYS:P 100 1 1) which took 5.14 minutes on an Intel(R) Core i7-2620M CPU at 2.70 GHz 32 bit operating system, are given in tab. 3.

Since 1 Sv = 100 rem, the neutron dose is ~6.3 10^{-9} rem h^{-1} for 1 source neutron per second; thus a neutron source of 10^8 s^{-1} would result in a (transmitted) neutron dose of 63 mrem h^{-1} compared with the ICRP recommended maximum of 20 mSv per year (2 rem per year or 0.22 mremh^{-1}). Without a water shield, a person at a distance 22 cm away would be receiving about 1000 times more *i. e*., ~ 63 remh^{-1}.

Table 3. Transmitted neutron and photon dose

F1:N	F2:N (Dose)	F1:P	F2:P (Dose)
Neutrons	Sv	Photons	Sv
1.67067 10^{-2} (0.0177)	4.10858 10^{-15} (0.0562)	1.6866 10^{-1} (0.0085)	1.6222 10^{-14} (0.0123)

The reaction rate $R_{H(n,\gamma)}$ from the F14:N tally is 2.94552 10^{-4} (0.0034) cm^{-3}; the total volume is 2200 cm^3 and thus $R_{H(n,\gamma)}$ = 0.6480 reactions per source neutron per second. Thus, for a source 10^8 neutrons per second, assuming one γ produced per radiative capture, the γ production in the water slab would be 0.6480 gammas per second. Less than 1% of these would be produced from group 1 (high energy) captures; thus the reaction rate is almost entirely from group 2 (lower energy) as expected from nuclear cross-section data.

It is seen from the MCNP5 results, in tab. 4, that a linearly decreasing density distribution (subject to constraint of fixed available material) gives an increase of ~4 % in the gamma production and ~1 % increase in the transmitted photon current and no significant increase (~<1 %) in the transmitted neutron current, compared with the uniform case. Out of all three, the decreasing density case leads to (a slight) enhanced photon production with enhanced transmittance.

Exact solutions were obtained for the two-group neutron fluxes, eq. 13(a) and eq. 13(b), for three cases *viz* $u(x)$ = const., $u(x) \sim 1/x$, and $u(x) \sim x$.

The group constants used for water are listed in tab. 5. In the present work, the data was obtained by using a *correction* factor in which $\sigma_{r,2}, \sigma_{tr,2}$ were modified to 0.5004 b and 90 b from 0.58869 b and 99.185 b, respectively, taken from Lamarsh and Barrata [17].

The molecular density of water in 3.3461 10^{22} molecules per cm^3 and, for case *i* (uniform density), the mean free paths are 2.9688 cm and 0.1107 cm, respectively, with D_1 = 1.13 cm, L_1 = 5.1961 cm, D_2 = = 0.1107 cm, L_2 = 2.5711 cm, $\tau \sim 27$ cm^2 and diffusion area ~6.61 cm^2. Further, to match DT and Monte Carlo results for the PI for case *i* (uniform distribution), $\sigma_{n\gamma}$ = = 87.475 b.

Since MCNP5 does not have options to generate group cross-sections [18], these two-group cross-sections can be obtained by using group fluxes ϕ_i and associated reaction rates $<\sigma_x\phi>$(where the inner product <…> implies integration over the energy group of interest), and setting the group cross-section, for group *i*, as $\sigma_x^{(i)}$ $\sigma_x\phi$ $/\phi_t$.

The existing methodology for obtaining multi-group cross-sections is based on reading ENDF pointwise cross-section data, by processing codes such as NJOY (LANL) and MC^2-3 (ANL) to produce binned cross-sections for use in multi-group deterministic codes. This is achieved by the group flux-weighting mentioned above and accounting for resonances and self-shielding.

The PI's for cases i-iii are

Table 4. Tallies for varying material distribution

$N(x)$	F1:N	Dose [Sv]	(n, g) avg [$cm^{-3}s^{-1}$]	F1:P
Decreasing	1.72933 10^{-2} (0.0174)	4.89229 $^{-15}$ (0.0580)	3.03990 10^{-4} (0.0033)	1.74480 10^{-1} (0.0084)
Uniform	1.71458 10^{-2} (0.0175)	4.25899 10^{-15} (0.0563)	3.00075 10^{-4} (0.0033)	1.71930 10^{-1} (0.0084)
Increasing	1.65803 10^{-2} (0.0180)	4.84695 10^{-15} (0.0605)	2.98457 10^{-4} (0.0033)	1.69710 10^{-1} (0.0085)

Table 5. Two-group cross-sections

Data/Group	1	2
σ_r [b]	1.2508	0.5004
σ_{tr} [b]	8.8158	90

$$PI_1 \quad N_0 \quad A_{31}L_2 e^{\frac{x}{L_2}} \quad A_{41}L_2 e^{\frac{x}{L_2}}$$

$$\bar{\omega}_0 A_{11}L_1 e^{\frac{x}{L_1}} \quad \bar{\omega}_0 A_{21}L_1 e^{\frac{x}{L_1}} \Big|_a^b \qquad (14a)$$

$$PI_2 \quad A \quad A_{32}\frac{x^{\beta_2}}{\beta_2} \quad A_{42}\frac{x^{\beta_2}}{\beta_2} \quad \varpi A_{12}\frac{x^{\beta_1}}{\beta_1}$$

$$\varpi A_{22}\frac{x^{\beta_1}}{\beta_1}\Big|_a^b \qquad (14b)$$

$$PI_3 \quad A \; A_3 I_3 \; \frac{\beta_2}{2} \quad A_4 I_3 \quad \frac{\beta_2}{2}$$

$$\bar{\omega}_2 \quad A_1 I_3 \; \frac{\beta_1}{2} \quad A_2 I_3 \quad \frac{\beta_1}{2} \qquad (14c)$$

where

$$\bar{\omega}_0 \quad \frac{\sigma_{r,1}}{\sigma_{r,2}} \; 1 \quad \frac{L_2}{L_1}^{2} \quad ^{1}, \quad \bar{\omega}_2 \quad \frac{\sigma_{r,1}}{\sigma_{r,2}} \; 1 \quad \frac{\beta_1}{\beta_2}^{2} \quad ^{1}$$

$$\beta_i \quad AN_0\gamma_i, A \quad 1/\ln b/a, \text{and } I_3(c) \quad \int_a^b xe^{cx^2}\,dx$$

Values of the PI from eqs. 14(a)-14(c) are given in tab. 6.

For the uniform case, the DT exact result matches well with the MCNP estimate $R_H(n,\gamma)$ = = 0.6480 reactions per source neutron per second, using the radiative capture cross-section σ_n =87.475 b. Further, the PI values for the theoretically limiting cases considered (cases ii and iii) show a relative decrease of about 2 % from the uniform distribution case. These estimates can be used to show, that there is only a very slight dependence of PI on the material distribution in this problem. However, the spatial distribution of the PI is seen to be dependent on the distribution of the material.

Table 6. Comparison of PI for varying $N(x)$

$N(x)$	PI
Lin. Dec.	0.63651
Uniform	0.64801
Lin. Inc.	0.63651

A situation of more practical significance is for mixtures of materials, where the optimal ratio of constituent elements is obtained, as for the enrichment in multiplying systems described in the previous section. Such applications arise for the radiation shielding surrounding nuclear systems. The size and design of such shields depends on the intensity and energy of the radiation as well as the material of the shield. Neutron shields are more effective and thus smaller in size, when the hydrogen content, as in water, is high while for photons, high atomic number materials such as iron and lead are preferred. The design proceeds along the following logic: slow the neutrons, then absorb, and finally absorb the gammas produced by the slowed neutrons (as in the $H(n, \gamma)$ reaction estimated in the previous section). A typical shield would thus consist of a hydrogenous or light atomic number material followed by a neutron absorber, such as boron, followed by a gamma shield. As an example, the half-value thickness of lead ($Z = 82$) for 1.0 MeV gamma radiation is ~0.76 cm which is half that of iron, which is about three times less than concrete while water is least effective of all these. Thus, for the last layer, lead would be thought to be the best choice.

Multilayered concrete shields

The design of multilayered concrete with aggregates (mainly gravel) is bound together by cement (mainly lime or calcium oxide, silica aluminium oxide) and water into a hard stone-like material with the required strength for structures such as buildings, bridges, roads *etc*. The relative composition of its constituents can be varied to provide the required mechanical *e. g*., the strength of concrete varies inversely with the mass ratio of water to cement. While Type 04 appears to be *representative* [19] with $\rho = 2.35$ gcm^{-3}, high-density concrete is made by mixing additives like scrap metal and magnetite. Piotrowski *et al*. [20] have carried out simulations for 25 cm thick wall of concrete of varying compressive strength to find that the effective dose behind the shield decreases up to 44 % as the compressive strength increases from 30 MPa (4351 psi) to 60 MPa (8702 psi) with water-cement (w-c) ratio 0.72 to 0.31. In other studies [21] the effect of boron in concrete has been studied to find that the optimal mixture of thermal neutron shielding concrete has a water-cement ratio of 0.38, cement content of 400 kgm^{-3}, a volume fraction Colemanite aggregate of 50 % and silica fume-cement ratio of 0.15.

Similarly, the effect of another strong absorber, gadolinium, has been studied [22] to find that in concrete Gd content up to 10 at.% concrete composite (10 cm × 5 cm thick) shielding efficiency of around 86 %). For multi-layered iron-water shields [23] the optimum arrangement reported is the thick iron-water-thin iron configuration, rather than a homogeneous mixture of iron and water layers. Optimization for shields has also been used with Genetic Algorithms [24] for the search for an optimal radiation shield configuration subject to a given set of constraints. A number of innovations such as nanomaterials in concrete have also been investigated [25].

Multi-layered detector shields

Another problem of practical application, is for detection systems for materials' identification by thermal neutron activation [26]. For such systems, ^{252}Cf has been used as a neutron source with emissions of 2.4 10^{12} s^{-1} g^{-1}. In detectors, especially portable detection systems, size and weight are crucial and hence an optimal design is of paramount importance. Light weight hydrogenous materials such as polyethylene, paraffin and water are thus good candidates for neutron shielding compared with heavy materials such as steel and lead.

The variational formulations presented are readily applicable for obtaining optimal radiation shield designs for the above cases.

CONCLUSIONS

In the first illustrative example for variational application in Monte Carlo, a two-zone optimality analysis yielded the condition for minimum critical mass with maximum fuel enrichment in the central zone and minimum enrichment in the outer zone. This information was used in a detailed Monte Carlo simulation which, in a single run, estimated first- and second-derivatives for prediction of k_{eff} for enrichment perturbations in both zones. These predicted estimates were subsequently used to estimate the minimum condition which was predicted to within 1 % of the re-run estimate, clearly demonstrating the benefit of using a variational estimate for computational enhancement of an elaborate MCNP simulation. Such an approach can, in principle, be used for larger problems.

In the second illustrative example, a continuous variational formulation was attempted to estimate the benefit of a non-uniform density distribution for a single material. It was found that an exact solution was not achievable and recourse would again be required for a discrete approach, as in the first example. However, it was possible to estimate the perturbation resulting from non-uniformity. The application of this approach to the design optimization of radiation shields was discussed.

Both examples illustrate the advantage in using preliminary variational results from two-group diffusion equations, as an initial guess in a MC perturbation strategy to yield reliable estimates.

NOMENCLATURE

b – barn (10^{-28}m^2)
D_i – diffusion coefficient for group i
H – Hamiltonian
i – energy group index
k_∞ – infinite multiplication factor
u – control variable
u' – enrichment
J – current, $J_i = -D_i \quad \phi_i$
L – slab width
L_i – diffusion length for group i
$\hat{L}_i$ – differential operator for energy group i
L^+ – adjoint operator
M – molecular (atomic) weight
$\hat{M}$ – two-group operator
N – atomic density
N_T – total number of atoms (=NV)
N_o – $\rho N_{av}/M$
N_{av} – Avogadro's number (6.023 10^{23} atoms/g-atom)
p – resonance escape probability
R_k – reaction rate for reaction type k
V – volume

Greek symbols

– Lagrange multiplier
$\mathcal{L}$ – Lagrangian
ρ – gram density
σ_k – microscopic cross-section for reaction k
– neutron age
ϕ_i – neutron flux for energy group i
ϕ_i – adjoint flux (Lagrange multiplier)
$_1$ – macroscopic scattering cross-section (group 1)
$_2$ – macroscopic absorption cross-section (group 2)
$_k$ – macroscopic cross-section for reaction k
$_{s,1\ 2}$ – macroscopic scattering cross-section grp 1 -> 2

Abbreviations

DT – diffusion theory
DTPMP – diffusion theory Pontryagin maximum principle
ENDF – Evaluated Nuclear Data File
F1:N/P – current tally for neutrons/photons
F2:N/P – surface flux tally for neutrons

ICRP – International Commission on Radiological Protection
NPS – number of particles simulated
PI – performance index
PMP – Pontryagin maximum principle
rem – Roentgen equivalent man (traditional unit)

AUTHORS' CONTRIBUTIONS

The mathematical modeling for variational and perturbation in the reactor core was carried out by Z. Koreshi and H. Khan, while the variational modeling for fixed-source was carried out by all three authors. Research was reviewed by all three authors.

REFERENCES

[1] Stacey, W. M., Jr., *Variational Methods in Nuclear Reactor Physics*, Academic Press, New York, USA, 1974
[2] Horie, J., Nishihara, H., Numerical Solution to Critical Problem of Finite Cylindrical Reactors by Variational Method, *Journal of Nuclear Science and Technology, 11* (1974), 9, pp. 358-368
[3] Lee, C. K., Critical Mass Minimization of a Cylindrical Geometry Reactor by Two-group Diffusion Equation, *Journal of the Korean Nuclear Society, 5* (1973), 2, pp. 115-131
[4] Conn, R., Stacey, W. M. Jr., Variational Methods for Controlled Thermonuclear Reactor Blanket Studies, *Nuclear Fusion, 13* (1973), 2, p. 185
[5] Graca, C. O., *et al*., Optimization of Blanket Design for Fusion Reactors by Higher Order Perturbation Theory, *Nuclear Energy, 27* (1988), 2, pp. 121-130
[6] Palmiotti, G., Salvatores, M., Developments in Sensitivity Methodologies and the Validation of Reactor Physics Calculations, *Science and Technology of Nuclear Installations, 2012* (2012), ID529623
[7] Lewis, E. E., The Variational Nodal Method: History & Recent Accomplishments, *Proceedings*, Congreso Internacional Conjunto Cancún LAS/ANS-SNM-SMSR /International Joint Meeting, Mexico, Cancun, 2004
[8] Palmiotti, G., *et al*., VARIANT: VARIational Anisotropic Nodal Transport for Multidimensional Cartesian and Hexagonal Geometry Calculation, Argonne National Laboratory, ANL-95/40, 1995
[9] Derstine, K. L., DIF3D: A Code to Solve One-, Two-, and Three-Dimensional Finite-Difference Diffusion Theory Problems, ANL-82-64, Argonne National Laboratory, 1984
[10] Lewis, F. L., *et al*., *Optimal Control*, 3rd Ed., John Wiley and Sons Inc., New York, USA, 2012
[11] Rief, H., Generalized Monte Carlo Perturbation Algorithms for Correlated Sampling and a Second-order Taylor Series Approach, *Annals of Nuclear Energy, 11* (1984), 9, pp. 455-476
[12] Koreshi, Z. U., Lewins, J. D., Two-group Monte Carlo Perturbation Theory and Applications in Fixed-Source Problems, *Progress in Nuclear Energy, 24* (1990), pp. 27-38
[13] Koreshi, Z. U., *et al*., Neutronic Sensitivity Analysis of the Experimental Test Reactor TIBER-II Blanket Design, *Fusion Technology, 22* (1992), 3, pp.371-387
[14] Kumar, A., Tsvetkov, P. V., A New Approach to Nuclear Reactor Design Optimization Using Genetic Algorithms and Regression Analysis, *Annals of Nuclear Energy, 85* (2015), Nov., pp 27-35
[15] Tengfei Zhang, *et al*., Acceleration of 3-D pin-by-pin Calculations Based on the Heterogeneous Variational Nodal Method, *Annals of Nuclear Energy, 114* (2018), Apr., pp. 165-174
[16] Briesmeister, J. F., Ed., MCNP – A General Monte Carlo N-Particle Transport Code, Version 4C, LA-13709-M, 2000
[17] Lamarsh, J. R., Baratta, A. J., *Introduction to Nuclear Engineering*, 3rd Ed., Prentice Hall, New Jersey, USA, 2001
[18] Hoogenboom, J., *et al*., Generation of Multi-Group Cross Sections and Scattering Matrices with the Monte Carlo Code MCNP5, *Proceedings*, Joint International Topical Meeting on Mathematics & Computation and Supercomputing in Nuclear Applications (M&C + SNA 2007) Monterey, Cal., USA, April 15-19, 2007
[19] Cacuci, D. G., *Handbook of Nuclear Engineering*, Springer, New York, USA, 2010
[20] Piotrowski, T., *et al*., Monte Carlo Simulations for Optimization of Neutron Shielding Concrete, *Central European Journal of Engineering, 2* (2012), 2, pp. 296-303
[21] Yadollahi, A., *et al*., Optimization of Thermal Neutron Shield Concrete Mixture Using Artificial Neural Networks, *Nuclear Engineering and Design, 305* (2016), Aug., pp. 146-155
[22] Park, J.-S., *et al*., Effects of Gadolinium in Fe Based Amorphous Ribbons with High Boron Contents on the Neutron Shielding Efficiency, *Annals of Nuclear Energy, 109* (2017), Nov., pp. 365-369
[23] Fuse, T., *et al*., The optimum Arrangement of Laminated Iron-Water Shields, *Nuclear Engineering and Design, 13* (1970), 3, pp. 390-394
[24] Kim, B. S., Hyun Moon, J., Use of a Genetic Algorithm in the Search for a Near-Optimal Shielding Design, *Annals of Nuclear Energy, 37* (2010), 2, pp. 120-129
[25] Norhasri, M., *et al*., Applications of Using Nano Material in Concrete: A review, *Construction and Building Materials, 133* (2017), Feb., pp. 91-97
[26] Khan, H., *et al*., The sensitivity studies of a landmine explosive detection system based on neutron backscattering using Monte Carlo simulation, *Nucl Technol Radiat, 32* (2017), 1, pp. 37-43

Received on February 14, 2109
Accepted on August 1, 2019

Зафар Улах КОРЕШИ, Хамда КАН, Мухамед ЈАКУБ

ВАРИЈАЦИОНИ МЕТОДИ И УБРЗАЊЕ МОНТЕ КАРЛО ПРОРАЧУНА ПЕРТУРБАЦИЈА РАДИ ОПТИМАЛНОГ ДИЗАЈНА НУКЛЕАРНИХ СИСТЕМА

Потрага за оптималном расподелом материјала у нуклеарном систему ради максимизације функције одзива од интереса, тема је од значаја у области нуклеарног инжењерства. Неки од примера су оптимална расподела горива у језгру нуклеарног реактора како би се остварило униформно сагоревање коришћењем минимума критичне масе, или примена композитних материјала са оптималном смешом градивних елемената у детекторским система или у заштити од зрачења. Варијационе методе корисне су за овакве прорачуне, али су коришћене само за појединачне анализе често ограничене на идеализоване моделе, док су за детаљније пројектовање биле потребне компјутерски захтевне Монте Карло симулације неподобне у итеративним оптимизационим шемама. Ова инхерентна мана Монте Карло метода промењена је са развојом пертурбационих алгоритама, али је њихова ефикасност и даље зависна од *референтне* конфигурације за коју се метода погоди-и-пробај често користи. У првом илустративном примеру у овом раду, испитује се убрзање прорачуна за голо цилиндрично језгро реактора, добијено применом варијационог резултата како би се побољшала ефикасност прорачуна Монте Карло симулација оптимизације дизајна. У другом примеру, приказан је утицај неуниформне густине материјала у фиксно позиционираном извору, који је примењив за прорачун оптималног модератора и заштиту од зрачења. Иако су употребе овог приступа бројне, циљ овог рада је да прикаже прелиминарне варијационе резултате као улазне податке за разраду стохастичке оптимизације Монте Карло симулација за велике и реалне системе.

Кључне речи: варијациона метода, оптимална расподела, Монте Карло пертурбација, нуклеарни систем, минимална критична маса